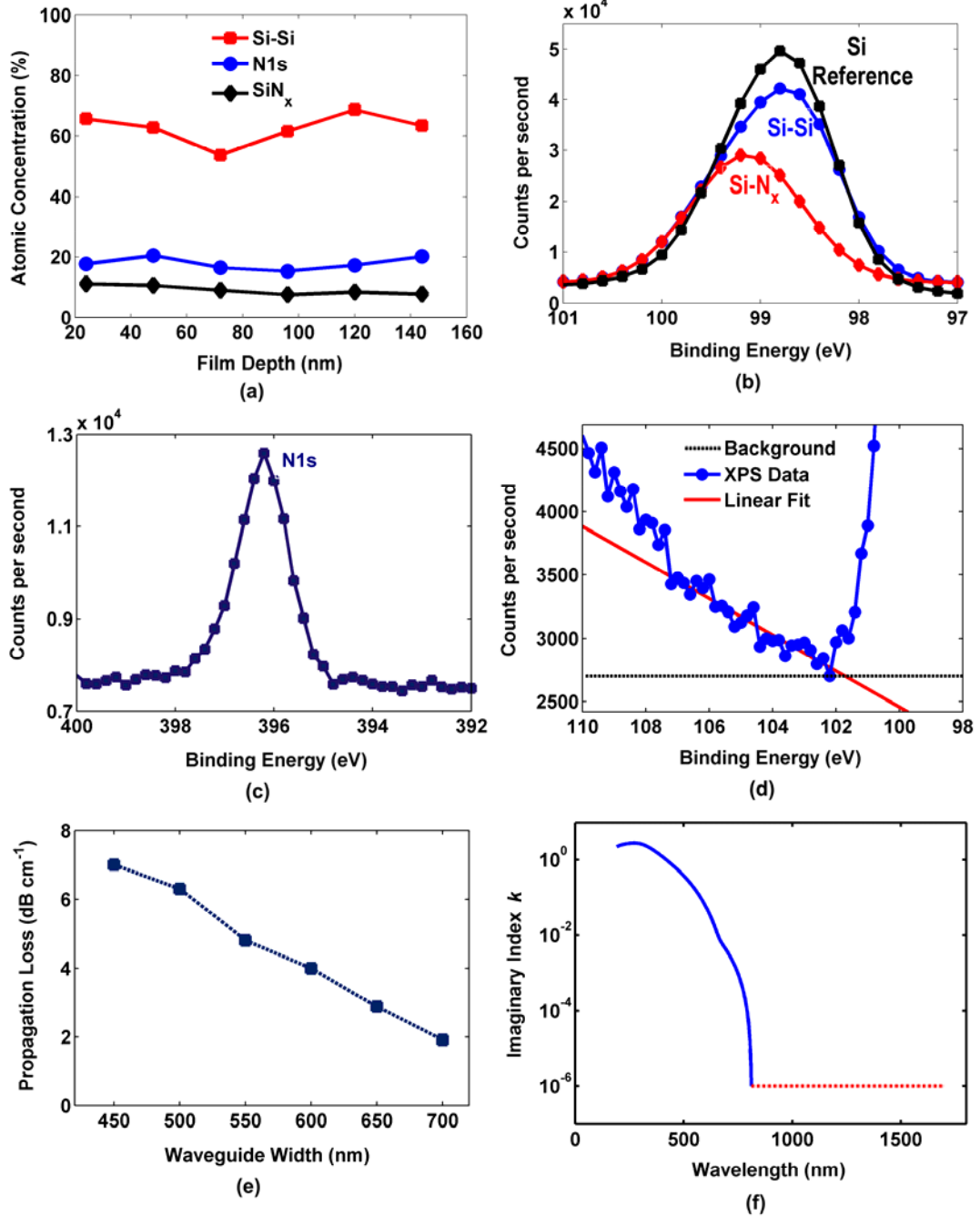


1

## SUPPLEMENTARY FIGURES



2

3

4 **Supplementary Figure 1. X-ray photoelectron spectroscopic characterization of the USRN**  
 5 **film.** (a) Atomic concentration of the Si-N, Si- Si and N1s bonds within the film, as a function  
 6 of film depth. (b) XPS Si 2p spectra of USRN film deconvoluted into two peaks. A pure Si film  
 7 is used as a reference for the Si-Si peak. (c) XPS N1s core-level spectrum of the USRN film. (d)  
 8 XPS spectrograph corresponding to inelastic collisions used to extrapolate the band gap  
 9 energy of the film. (e) Measured waveguide propagation losses as a function of the waveguide  
 width with improved losses. The propagation losses decrease as waveguide

10 width is increased, suggesting that sidewall roughness plays a big role in the measured  
11 propagation losses. (f) Measured material loss of USRN. The lowest measurable  $k$  value is  $10^6$   
12 or  $0.35 \text{ dB cm}^{-1}$ . Material loss from wavelength 810 nm to 1700 nm is below the detection  
13 limit (red dashed line).

14

## 15 SUPPLEMENTARY NOTE 1

16 Supplementary Figure 1a shows the plot of the atomic concentration of USRN taken  
17 using X-ray photoelectron spectroscopy (XPS) from a depth of 20 nm to 140 nm into  
18 the film. The measurement detects the presence of Si and N with a higher percentage  
19 of Si concentration. The ratio of Si:N is extracted to be approximately 7:3, which is  
20 close to that which was detected by energy dispersive X-ray spectroscopy. Previous  
21 characterization using EDX measurements were sufficient mainly to determine the  
22 presence of higher amount of Si compared to N in the silicon-rich nitride film and to  
23 estimate the Si:N ratio. Further characterization using XPS performed here provides a  
24 more accurate measurement on the film composition compared to EDX as it uses a  
25 monochromatic Al K-alpha X-ray source under high vacuum to obtain the film's  
26 chemical compositions and more importantly, the binding energies. By X-ray  
27 bombardment, core electrons in the film are excited and therefore freed from the  
28 nucleus attractive force. Once the electrons are in the vacuum, they are collected by  
29 an electron analyzer. The XPS spectrum is obtained by counting the number of  
30 electrons versus their binding energy.

31 Apart from the percentages of Si and N in the film, an important result obtained  
32 through XPS characterization is the exact binding energy of the USRN films, and  
33 determines that Si-Si and Si-N bonding did indeed occur in the film. Supplementary  
34 Figure 1b shows the XPS binding energies' narrow scan from 97-101 eV alongside a  
35 reference measurement using a pure Si film sample. Taking the Si-Si peak (98.7 eV)  
36 as a reference, USRN film is further deconvolved into two curves at 98.7 eV (Si-Si  
37 peak) and 99.2 eV. This indicates that the USRN film consists of an Si-Si peak and a  
38 second peak. As this second peak occurs at neither  $\text{Si}_3\text{N}_4$  (101.8 eV)<sup>1</sup> nor  $\text{SiO}_2$  (103.6  
39 eV)<sup>2</sup> and atomic concentration (Supplementary Figure 1a) reveals presence of Si and  
40 N, we believe that this second peak is attributed to the Si-N<sub>x</sub> bonding in the film.  
41 Furthermore, a narrow scan from 392-400 eV reveals an N1s peak at approximately  
42 396.2 eV (Supplementary Figure 1c), which corresponds to the typical N1s peak of  
43 Si-N (Ref. 3), further evidence that Si-N bonds indeed exist in our films. The presence  
44 of Si-Si, N1s and Si-N bonds in the indicated percentages suggests that the film  
45 possesses bonds which are similar to that of stoichiometric silicon nitride films, but  
46 with a comparatively larger amount of Si-Si, thus confirming the silicon-rich nature of  
47 our films.

48 Energy losses observed via X-ray photoelectron spectroscopy enable the energy band  
49 gap of the silicon rich nitride film to be extrapolated<sup>3</sup>. Inelastic scattering from surface  
50 plasmons induced by photoexcited electrons generate an energy loss equivalent to the  
51 material's energy band gap. This reduction in kinetic energy manifests itself as a  
52 broad peak with an increased binding energy relative to the location of the  
53 characteristic bond's elastic peak. The band gap energy can therefore be derived from

54 the difference between the location of the elastic peak, and that where inelastic  
55 collisions are observed to occur in the XPS spectrograph. Supplementary Figure 1d  
56 shows the XPS spectrograph of our USRN film used to extrapolate the band gap  
57 energy, where the onset of inelastic collisions occurs. The intersection point between  
58 the background level of the measurement and the linear fit to the slope immediately  
59 preceding the Si-N peak represents the upshift in binding energy relative to the Si-N  
60 peak as a result of inelastic collisions. The difference between this intersection point  
61 and the Si-N peak gives us the band gap energy of the film, determined to be 2.1 eV.  
62 This band gap energy is large enough to eliminate two-photon absorption at 1550 nm,  
63 including those from Urbach tails which are characteristic of amorphous films, and  
64 places the film well above the two photon absorption edge. From Supplementary  
65 Figure 1a, it is also observed that the Si:N ratio stays relatively constant at various  
66 film depths, implying that our films are homogeneous. This property is important to  
67 ensure that the material's nonlinearity effectively interacts uniformly with the  
68 waveguide mode residing within the USRN core. Further, optical characterization of  
69 the films'  $n-k$  values has revealed that our films possess a relatively large linear  
70 refractive index of 3.1 at 1550 nm (Ref. 4), and allows for significant design freedom  
71 to engineer varying magnitudes and signs of waveguide dispersion, a feature which is  
72 important for many nonlinear optics phenomena such as four-wave mixing and optical  
73 pulse compression. The nonlinear Kerr coefficient was previously evaluated to be  
74  $2.8 \times 10^{-13} \text{ cm}^2 \text{ W}^{-1}$  (Ref. 4). This nonlinear parameter is slightly higher than that in  
75 silicon waveguides, and two orders of magnitude larger than that in silicon nitride,  
76 silicon-rich nitride waveguides (with a refractive index  $\leq 2.2$ ) and Hydex waveguides,  
77 which when coupled with the large band gap characterized using XPS to be 2.1 eV,  
78 implies a high nonlinear figure of merit at 1550 nm.

79

80

81

82

83

84 **SUPPLEMENTARY REFERENCES**

- 85 1. Lee, W. J. & Kim, U. J. Characteristics of silicon nitride thin films prepared by using  
86 alternating exposures of  $\text{SiH}_2\text{Cl}_2$  and  $\text{NH}_3$ . *J. Korean Phys. Soc.* **47**, S598-S602 (2005).
- 87 2. Ulrich, M. D. *et al.* Soft X-ray photoelectron spectroscopy of  $(\text{HfO}_2)_x(\text{SiO}_2)_{1-x}$  high-*k*  
88 gate-dielectric structures. *J. Vac. Sci. Technol. B* **21**, 1777-1782 (2003).
- 89 3. Goto, T. & Hirai, T. J. ESCA study of amorphous CVD  $\text{Si}_3\text{N}_4$ -BN composites. *J. Mater.*  
90 *Sci. Lett.* **7**, 548-550 (1988).
- 91 4. Wang, T. *et al.* Supercontinuum generation in bandgap engineered, back-end CMOS  
92 compatible silicon rich nitride waveguides. *Laser Photon. Rev.* **9**, 498-506 (2015).

93

94